Received: 27 March 2025 | Revised: 22 June 2025 | Accepted: 31 July 2025

DOI: 10.1002/aic.70030

AIChE JOURNAL

RESEARCH ARTICLE

Biomolecular Engineering, Bioengineering, Biochemicals, Biofuels, and Food

Cuprous ionic liquid engineering combined with preorganized hydrogen-bond donors for enhanced carbon monoxide capture

Guokai Cui[1] | Chengyu Ren[1] | Ruina Zhang[1] | Xing Li[1] | Zhenzhen Yang[2] | Lei Zhang[1] | Quanli Ke[1] | Ying Zhou[1] | Hanfeng Lu[1] | Sheng Dai[2,3]

[1]Innovation Team of Air Pollution Control, Institute of Catalytic Reaction Engineering, Zhejiang Key Laboratory of Surface and Interface Science and Engineering for Catalysts, State Key Laboratory of Green Chemical Synthesis and Conversion, College of Chemical Engineering, Zhejiang University of Technology, Hangzhou, China

[2]Chemical Sciences Division, Oak Ridge National Laboratory, Oak Ridge, Tennessee, USA

[3]Department of Chemistry, Institute for Advanced Materials and Manufacturing, University of Tennessee, Knoxville, Tennessee, USA

Correspondence
Guokai Cui and Hanfeng Lu, Innovation Team of Air Pollution Control, Institute of Catalytic Reaction Engineering, Zhejiang Key Laboratory of Surface and Interface Science and Engineering for Catalysts, State Key Laboratory of Green Chemical Synthesis and Conversion, College of Chemical Engineering, Zhejiang University of Technology, Hangzhou 310014, China.
Email: chemcgk@163.com and luhf@zjut.edu.cn

Sheng Dai, Chemical Sciences Division, Oak Ridge National Laboratory, Oak Ridge, TN 37831, USA.
Email: dais@ornl.gov

Funding information
Key Research and Development Projects in Zhejiang Province, Grant/Award Numbers: 2024C03108, 2023C03127, 2024C03114; National Natural Science Foundation of China, Grant/Award Numbers: 22378353, 22208300; Zhejiang Provincial Natural Science Foundation of China, Grant/Award Number: LTGS24E080008; Zhejiang Provincial Postdoctoral Science Foundation, Grant/Award Number: ZJ2023145; Division of Chemical Sciences, Geosciences, and Biosciences, Office of Basic Energy Sciences, US Department of Energy

Abstract

Carbon monoxide (CO) is a toxic but valuable precursor for organic synthesis. Thus, CO capture is an important and sustainable process. Here, a strategy of cuprous ionic liquid engineering combined with preorganized hydrogen-bond donors (HBDs) was first developed to form a series of functional deep eutectic solvents (DESs) for enhanced CO capture via promoting cooperation, and the stepped sorption isotherms with a characteristic threshold "gate-opening" pressure were obtained. It was found that the enhanced absorption capacity (up to 220%) and enhanced working capacity (up to 310%) can be reached by DESs with preorganized HBDs. Quantum-chemical calculations and spectroscopic investigations revealed that cooperative interactions and preorganized benzenediols were the reason for equimolar capacities. Additionally, at least 17 absorption–desorption cycles with high CO capacity could be reached, indicating excellent reversibility. Thus, easy preparation, high Cu(I) efficiency, and high working capacity make these DESs an alternative way for CO capture.

KEYWORDS
benzenediol, CO sorption, coordination, cuprous, deep eutectic solvents, ionic liquids

1 | INTRODUCTION

Carbon monoxide (CO) is not only harmful to human health due to its high toxicity but also detrimental to catalysts in proton-exchange-membrane fuel cells as an impurity gas in H_2, which is generated simultaneously by steam reforming of natural gas/coal gasification. On the other hand, pure CO is a resource and can be transferred to value-added chemicals via carbonylation reactions[1] and electroreduction reactions,[2] or presents a potential clinically viable medicinal agent.[3] Therefore, CO capture is an important and sustainable process in CO separation and H_2 production.[4,5] The conventional cuprous aluminium chloride (CuAlCl4) complex in toluene solution (COSORB) process for CO capture results in the low capacity of CO, the low stability of the complex, and the loss of toluene as an organic solvent.[6]

Because the high solubility of CO in sorbent is very beneficial to improving the separation selectivity and the reaction rates, developing alternative clean and sustainable technologies for highly efficient and reversible CO removal is important.[7]

Ionic liquids (ILs),[8–11] formed by cations and anions, and deep eutectic solvents (DESs),[12–14] formed by hydrogen-bond accepters (HBAs) and hydrogen-bond donors (HBDs), as two kinds of solvents, have received a lot of attention in recent decades with similar tunable physical–chemical properties, such as low vapor pressure, high thermal and chemical stability, and high solubilization for the capture of gases such as NO_x,[14–17] CO_2,[18–27] SO_2,[28–34] NH_3,[35–38] H_2S[39–43] etc. Through structural regulation, functionalized ILs and DESs with active sites could obtain high CO capacity compared to conventional ILs and DESs.[44] Laurenczy et al.[45] reported the first solubility of CO in the conventional ILs according to [Bmim][BF_4] < [Bmim][PF_6] < [Bmim][SbF_6] < [Bmim][CF_3COO] < [Bmim][Tf_2N]. Tao et al.[46] showed a CO capacity of up to 0.046 mol CO per mol IL by [P_{4448}][Pen] at 25°C and 1 bar. Considering the coordination of Cu(I) in CO capture,[47] Cu(I)-based ILs were reported with different efficiencies of Cu(I). For example, [Hmim][$CuCl_2$],[48] triethylammonium dichlorocuprate(I) [TEA][$CuCl_2$],[49] and 1-ethylimidazolium dichlorocuprate(I) [EimH][$CuCl_2$][50] were reported with CO capacities of 0.020, 0.078, and 0.118 mol CO per mol Cu(I) at 303.2 K and 1 bar, respectively. Cui et al.[51] reported a capacity of 0.203 mol CO per mol Cu(I) for [HDEEA][Cl] + CuCl + ethylene glycol (EG) (1:1:4) at 20°C and 1 bar. Peng et al.[52] showed that N, N, N', N'-tetramethyl-N-hexyl-1,5-ethyletherdiammonium bis[trichlorodicuprate (I)] [HBDMAEE-C_6][Cu_2Cl_3]$_2$ reached 0.063 mol CO per mol Cu(I) at 313.2 K and 1 bar. Although Cu(I)-based sorbents showed higher CO capacities than those of conventional Cu(I)-free sorbents, the capacity of CO and the efficiency of Cu(I) are still lower than the maximum saturation described by a 1:1 stoichiometric ratio, meaning that most Cu(I) are inactivated and difficult for CO capture under atmospheric pressures. How to develop novel functional solvents to achieve high efficiency of Cu(I) and high working capacity of CO is still a challenging task.

Herein, a strategy of cuprous ionic liquid engineering combined with preorganized HBDs was developed to form a series of functional DESs for enhanced CO capture. First, we designed and prepared a series of DESs with Cu(I)-based IL [CMPyH][$CuCl_2$] as HBA and diol compounds, such as EG and 1,3-propanediol (PD) as well as preorganized *o*-dihydroxybenzene (*o*-DHB) and *m*-dihydroxybenzene (*m*-DHB) as HBDs at different molar ratios (1:1, 1:1.5, and 1:2). Then, high Cu(I) efficiency (up to 0.921 mol CO per mol Cu(I)) could be reached at 20°C and 5 bar CO via tuning the structures and molar ratios of HBA:HBD. Additionally, compared with alkanediols, the cooperative interactions of Cu(I) and preorganized benzenediols in DESs with CO were the reason for equimolar capacities (Figure 1).

2 | EXPERIMENTAL METHODS

2.1 | Materials

Solvents, reagents, and chemicals are purchased from commercial suppliers and used without further purification. 2-(Chloromethyl)pyridine hydrochloride ([CMPyH][Cl], 98.0%), copper(I) chloride (CuCl, 97.0%) and *o*-DHB (99.5%) were purchased from Shanghai Aladdin Biochemical Technology Co., Ltd. EG (99.0%) was supplied by Sinopharm Chemical Reagent Co., Ltd., while PD (98.0%) and *m*-DHB (99.5%)

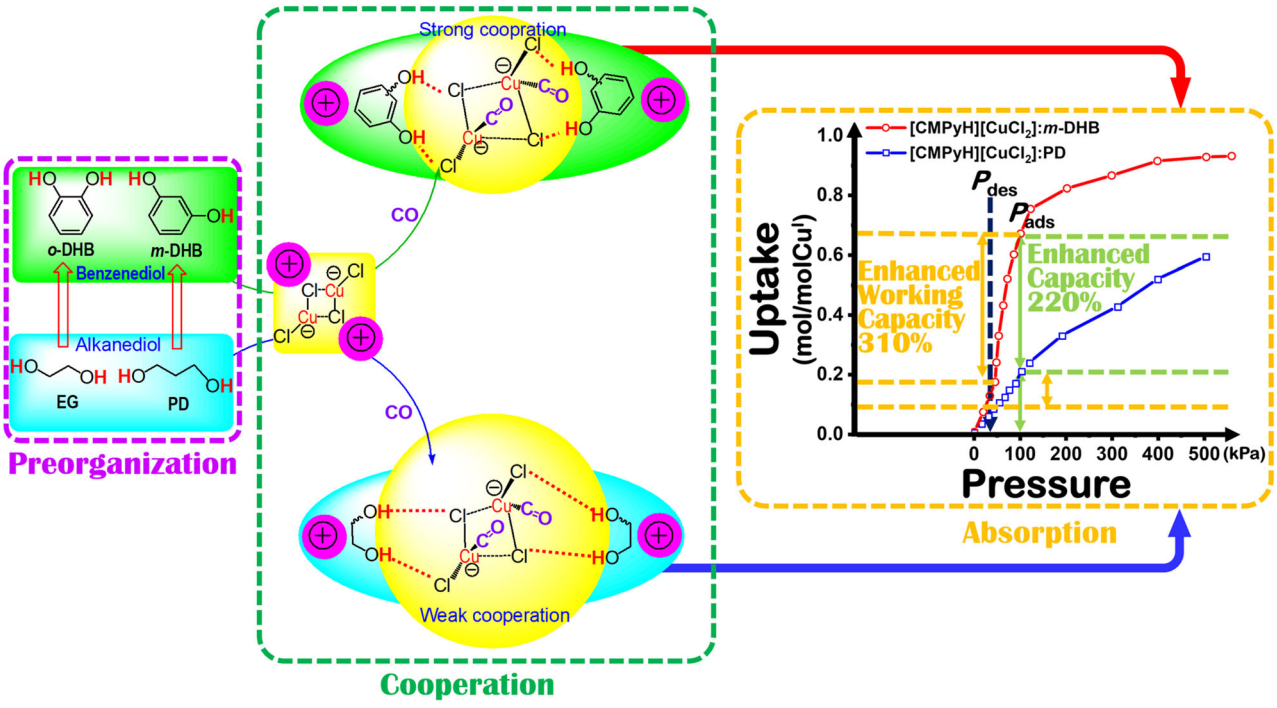

FIGURE 1 Cuprous ionic liquid engineering combined with preorganized hydrogen-bond donors for enhancing the working capacity of carbon monoxide (CO) via cooperation. EG, thylene glycol; *m*-DHB, *m*-dihydroxybenzene; *o*-DHB, *o*-dihydroxybenzene; PD, 1,3-propanediol.

were obtained from Shanghai Macklin Biochemical Co., Ltd. CO (99.99%) and nitrogen (N_2, 99.99%) were purchased from Hangzhou Jingong Special Gas Co., Ltd.

2.2 | Preparation of DESs

Taking the preparation of 2-(chloromethyl) pyridinium dichlorocuprate (I) [CMPyH][$CuCl_2$]:*o*-DHB (1:1) as an example, the DES was synthesized via two steps. Firstly, a certain amount of liquid [CMPyH][Cl] was mixed with an equal molar amount of solid CuCl at 80°C under N_2 for 0.5 h to obtain transparent liquid [CMPyH][$CuCl_2$]. Then, [CMPyH][$CuCl_2$] as a HBD was mixed with the same molar ratio of *o*-DHB at 80°C for 3 h, and readily the target IL-based DES [CMPyH][$CuCl_2$]:*o*-DHB(1:1) was prepared.

2.3 | Characterization and physical properties of DESs

Fourier transform infrared spectrometer (FT-IR) spectra were measured with a scanning wavelength range of 4000–400 cm^{-1} by VERTEX-70 FT-IR of Bruker, a German company. ^{13}C Nuclear magnetic resonance spectrometer (NMR) spectra were recorded using d_6-DMSO as a solvent on an AVANCE 400 NMR, and the residual dimethylsulfoxide (DMSO) signal ($\delta = 39.5$ ppm) was selected as the reference. Densities of DESs were carefully determined using a pycnometer at T = (20, 30, 40, 50, 60, 70, and 80°C) with an accuracy of ±0.1°C under atmospheric pressure via the specific gravity bottle method, using the definition of density following the equation:

$$\rho = \frac{(m_1 - m_0)}{V_0},$$

where m_1 in g is the total mass of gravity bottle and DES, V_0 in cm^3 is the gravity bottle in the temperature volume of the volumetric bottle, ρ is the density of DES. The viscosity of the DESs was also measured by a Brookfield (DVNEXT-LV) viscometer at aforementioned temperatures.

2.4 | CO capture by DESs

CO capture experimental device could be found in Figure 2, which composes two 316 L stainless steel high-sealing tanks. The larger tank is a gas storage tank, which is used to temporarily store CO gas, while the smaller tank is a gas absorption tank for CO capture by DES (~2 mL). The temperature is controlled by the thermostatic water bath device. The pressure (<600 kPa) is monitored in real time by the pressure sensor, which is connected to the digital display instrument for data recording in real time. When the pressure in the absorption tank no longer changes within 2 h, the CO absorption in DES reaches a two-phase equilibrium state under certain temperature and CO

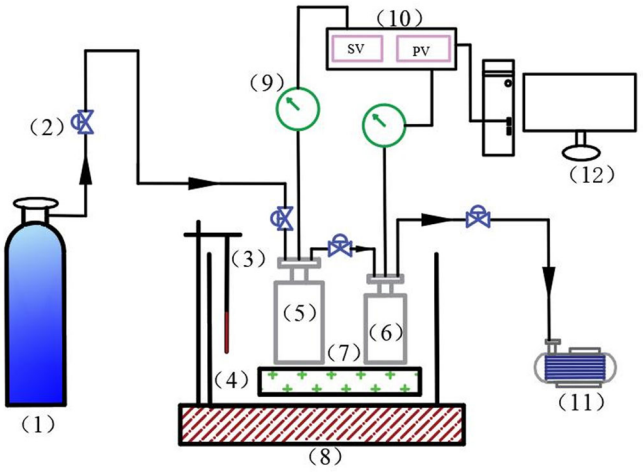

FIGURE 2 Carbon monoxide (CO) capture equipment. (1) CO gas cylinder, (2) high pressure horizontal valve, (3) thermocouple, (4) water bath, (5) gas storage tank, (6) gas absorption tank, (7) thermostatic device, (8) magnetic agitator, (9) pressure sensor, (10) digital display instrument, (11) vacuum pump, (12) computer.

partial pressure conditions. The CO capture capacity can be calculated via the following equation:

$$n(P_S) = \rho_{CO}(P_1, T)V_1 - \rho_{CO}(P'_1, T)V_1 - \rho_{CO}(P_g, T)(V_2 - V_{DES}),$$

where $\rho_{CO}(P_1, T)$, $\rho_{CO}(P'_1, T)$ and $\rho_{CO}(P_S, T)$ refer to the density of CO in mol cm^{-3} at partial pressures P_1, P'_1, and P_g, respectively, and temperature T, while V_1, V_2, and V_{DES} represent the volumes in cm^3 of the gas storage tank, the absorption tank, and the DES absorbent, respectively. P_1 and P'_1 are the record CO partial pressures of the gas storage tank before and after the purge of CO into the absorption tank. P_s is the equilibrium pressure of CO in the absorption tank, and $P_g = P_2 - P_0$, where P_2 and P_0 are the record CO partial pressures of the absorption tank before and after the absorption of CO in DES. The averaged uncertainty of solubility data in this work was within ±0.1%.

3 | RESULTS AND DISCUSSION

3.1 | Physical properties of DESs

The density (ρ) in g cm^{-3} and the viscosity (η) in mPa s are two important physical properties of DESs. The density and viscosity of these DESs with different HBDs and molar ratios were measured in the range of 20–80°C, and the data are shown in Tables 1 and 2, respectively. It is clear that the density of each DES decreased with the increase in temperature. The linear equation was used to study the relationship of density vs. temperature as follows:

$$\ln\rho = a + bT,$$

where a and b are fitting parameters, and their values were collected in Table 3. Figure 3 shows the plotted ln ρ vs. T (R^2 >0.99). However,

TABLE 1 Densities (ρ, in g cm^{-3}) of prepared deep eutectic solvents (DESs) at different temperatures.

	Temperature (°C)						
DES	20	30	40	50	60	70	80
[CMPyH][$CuCl_2$]:EG (1:1)	1.6022	1.5960	1.5882	1.5795	1.5730	1.5674	1.5614
[CMPyH][$CuCl_2$]:EG (1:1.5)	1.5545	1.5495	1.5402	1.5340	1.5279	1.5207	1.5133
[CMPyH][$CuCl_2$]:EG (1:2)	1.5186	1.5086	1.4983	1.4834	1.4749	1.4615	1.4530
[CMPyH][$CuCl_2$]:*o*-DHB (1:1)	1.5975	1.5853	1.5756	1.5663	1.5541	1.5458	1.5331
[CMPyH][$CuCl_2$]:*o*-DHB (1:1.5)	1.5282	1.5244	1.5174	1.5096	1.5035	1.4972	1.4924
[CMPyH][$CuCl_2$]:*o*-DHB (1:2)	1.4956	1.4887	1.4770	1.4700	1.4602	1.4502	1.4421
[CMPyH][$CuCl_2$]:PD (1:1)	1.5351	1.5301	1.5225	1.5155	1.5105	1.5034	1.4983
[CMPyH][$CuCl_2$]:PD (1:1.5)	1.4655	1.4579	1.4536	1.4457	1.4389	1.4314	1.4252
[CMPyH][$CuCl_2$]:PD (1:2)	1.4277	1.4159	1.4058	1.3979	1.3889	1.3793	1.3685
[CMPyH][$CuCl_2$]:*m*-DHB (1:1)	1.5784	1.5726	1.5685	1.5644	1.5568	1.5509	1.5469
[CMPyH][$CuCl_2$]:*m*-DHB (1:1.5)	1.5539	1.5401	1.5301	1.5212	1.5073	1.4978	1.4852
[CMPyH][$CuCl_2$]:*m*-DHB (1:2)	1.5205	1.5121	1.5011	1.4914	1.4812	1.4702	1.4588

Abbreviations: EG, thylene glycol; *m*-DHB, *m*-dihydroxybenzene; *o*-DHB, *o*-dihydroxybenzene; PD, 1,3-propanediol.

TABLE 2 Viscosities (η, in mPa s) of prepared deep eutectic solvents (DESs) at different temperatures.

	Temperature (°C)						
DES	20	30	40	50	60	70	80
[CMPyH][$CuCl_2$]:EG (1:1)	216.9	84.59	44.49	27.02	17.97	12.57	9.68
[CMPyH][$CuCl_2$]:EG (1:1.5)	138.5	61.23	33.04	20.31	13.55	9.800	7.64
[CMPyH][$CuCl_2$]:EG (1:2)	90.44	44.44	24.92	15.82	10.73	7.830	6.36
[CMPyH][$CuCl_2$]:*o*-DHB (1:1)	4806	1252	346.9	190.3	97.57	53.64	34.22
[CMPyH][$CuCl_2$]:*o*-DHB (1:1.5)	3442	902.91	323.61	140.25	71.84	42.23	27.18
[CMPyH][$CuCl_2$]:*o*-DHB (1:2)	2350	673.1	235.9	107.8	60.19	35.19	24.17
[CMPyH][$CuCl_2$]:PD (1:1)	427.7	165.5	77.68	47.82	32.96	24.22	18.55
[CMPyH][$CuCl_2$]:PD (1:1.5)	347.4	111.1	60.39	40.16	27.53	20.85	16.96
[CMPyH][$CuCl_2$]:PD (1:2)	199.8	81.85	43.53	28.51	20.89	17.32	14.10
[CMPyH][$CuCl_2$]:*m*-DHB (1:1)	5930	1534	495.1	217.2	104.4	59.47	36.46
[CMPyH][$CuCl_2$]:*m*-DHB (1:1.5)	5273	1330	472.1	197.4	101.3	59.47	35.81
[CMPyH][$CuCl_2$]:*m*-DHB (1:2)	3893	1031	352.8	152.4	81.14	45.08	30.51

Abbreviations: EG, thylene glycol; *m*-DHB, *m*-dihydroxybenzene; *o*-DHB, *o*-dihydroxybenzene; PD, 1,3-propanediol.

the density data were all in the range of 1.35–1.6 g cm^{-3}. indicating that the impact is not significant. Besides, the density of DES was affected by the molar ratio of HBA to HBD. For example, the densities of [CMPyH][$CuCl_2$]:*o*-DHB (1:1), [CMPyH][$CuCl_2$]:*o*-DHB (1:1.5), and [CMPyH][$CuCl_2$]:*o*-DHB (1:2) at 20°C were measured to be 1.5975, 1.5282, 1.4956 g cm^{-3}, respectively, indicating that the density of DESs decreased with the increase in the amount of HBDs, and the densities of HBDs were lower than that of [CMPyH][$CuCl_2$]. Additionally, the thermal expansion coefficient (α_p, in K^{-1}) values reflect the free volume of DES, and high α_p leads to a high free volume of DES. α_p can be calculated by:

$$\alpha_p = \frac{1}{V} \times \left(\frac{\partial V}{\partial T}\right)_p = -\left(\frac{\partial \ln \rho}{\partial T}\right)_p,$$

where V is molar volume of DES in cm^3 mol^{-1}. Clearly, $-b$ equals α_p, and α_p for [CMPyH][$CuCl_2$]:EG (1:2), [CMPyH][$CuCl_2$]:*o*-DHB (1:2), [CMPyH][$CuCl_2$]:PD (1:2), and [CMPyH][$CuCl_2$]:*m*-DHB (1:2) were 7.5591×10^{-4}, 6.1830×10^{-4}, 6.8449×10^{-4}, and 6.9222×10^{-4} K^{-1}, respectively.

The viscosity of typical DES was affected by temperature, HBDs, and molar ratios, and the data were measured and shown in Table 2. The viscosity of each DES also decreased with the increase of temperature. For example, the viscosity of [CMPyH][$CuCl_2$]:EG (1:1.5) decreased from 138.5 to 7.64 mPa s with the increase of temperature from 20 to 80°C. The temperature has a great influence on the viscosity of the DESs based on preorganized HBDs. The viscosity of [CMPyH][$CuCl_2$]:*o*-DHB (1:1.5) decreased from 3442 to 27.18 mPa s with the increase of temperature

TABLE 3 Fitting parameters for equations $\ln \rho = a + bT$ and $\ln\eta = \ln\eta_0 + (E_\eta/RT)$.

DES	Parameters for $\ln \rho = a + bT$			Parameters for $\ln\eta = \ln\eta_0 + (E_\eta/RT)$		
	a	b ($\times 10^4$)	R^2	η_0	E_η	R^2
[CMPyH][$CuCl_2$]:EG (1:1)	0.6002	−4.3988	0.99568	2.798×10^6	43.6	0.97579
[CMPyH][$CuCl_2$]:EG (1:1.5)	0.5736	−4.5045	0.99862	5.330×10^6	41.1	0.98042
[CMPyH][$CuCl_2$]:EG (1:2)	0.6399	−7.5591	0.99672	1.431×10^5	36.2	0.97979
[CMPyH][$CuCl_2$]:*o*-DHB (1:1)	0.6646	−6.7071	0.99807	1.316×10^9	69.6	0.97561
[CMPyH][$CuCl_2$]:*o*-DHB (1:1.5)	0.5466	−4.1545	0.99483	1.379×10^9	68.8	0.98152
[CMPyH][$CuCl_2$]:*o*-DHB (1:2)	0.5844	−6.1830	0.99757	4.035×10^9	65.28	0.97842
[CMPyH][$CuCl_2$]:PD (1:1)	0.5501	−4.1308	0.99745	4.696×10^6	43.98	0.96448
[CMPyH][$CuCl_2$]:PD (1:1.5)	0.5188	−4.6593	0.99709	1.081×10^5	41.18	0.94402
[CMPyH][$CuCl_2$]:PD (1:2)	0.5506	−6.8449	0.99769	4.013×10^5	36.8	0.94594
[CMPyH][$CuCl_2$]:*m*-DHB (1:1)	0.5569	−3.4198	0.99311	5.430×10^{10}	72.4	0.98363
[CMPyH][$CuCl_2$]:*m*-DHB (1:1.5)	0.6564	−7.3703	0.99738	1.017×10^9	70.5	0.98254
[CMPyH][$CuCl_2$]:*m*-DHB (1:2)	0.6229	−6.9222	0.99826	1.319×10^9	69.2	0.98024

Abbreviations: DES, deep eutectic solvents; EG, thylene glycol; *m*-DHB, *m*-dihydroxybenzene; *o*-DHB, *o*-dihydroxybenzene; PD, 1,3-propanediol.

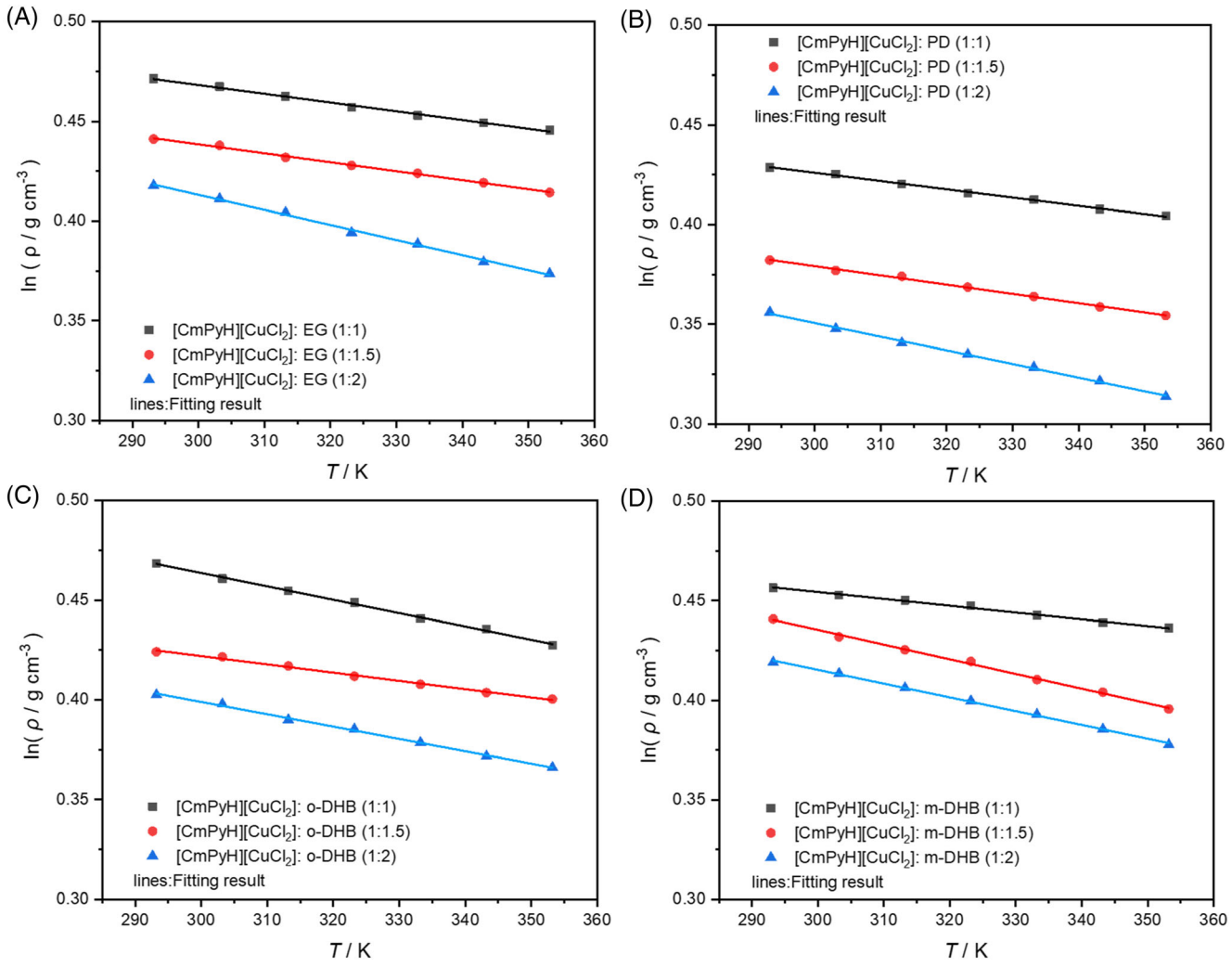

FIGURE 3 Linear relationship of lnρ vs. T for deep eutectic solvents with different hydrogen-bond donors. (A) Ethylene glycol (EG), (B) 1,3-propanediol (PD), (C) *o*-dihydroxybenzene (*o*-DHB), (D) *m*-dihydroxybenzene (*m*-DHB).

from 20 to 80°C. The relationship of viscosity vs. temperature was correlated by the Arrhenius equation, $\ln\eta = \ln\eta_0 + E_\eta/(RT)$, where η_0 in mPa s represents the pre-exponential constant, E_η in kJ mol^{-1} is the flow activation energy of DES, and $R = 8.314$ J mol^{-1} K^{-1}. Figure 4 shows the plotted ln η vs. $1/T$ (R^2 >0.9), and the values of parameters were also listed in Table 3. The values of E_η for [CMPyH][$CuCl_2$]:EG (1:2), [CMPyH][$CuCl_2$]:*o*-DHB (1:2), [CMPyH][$CuCl_2$]:PD (1:2), and [CMPyH][$CuCl_2$]:*m*-DHB (1:2) were calculated to be 36.2, 65.28, 36.8, and 69.2 kJ mol^{-1}, respectively. In general, an increase in the flow activation energy (from alkanediol HBDs to benzenediol HBDs) corresponds with an increased influence of the temperature on the viscosity. The difference between the structures of alkanediol HBDs and benzenediol HBDs is the benzene ring, leading to the high activity of hydroxyl groups in the benzenediol HBDs. It can be seen that the viscosities of [CMPyH][$CuCl_2$]:EG (1:2) and [CMPyH][$CuCl_2$]:*o*-DHB (1:2) at 20°C were measured to be 90.44 and 2350 mPa s, respectively, due to the weak hydrogen-bond network in the former and strong hydrogen-bond network in the latter. For the comparison of [CMPyH][$CuCl_2$]:*o*-DHB (1:2) and [CMPyH][$CuCl_2$]:*m*-DHB (1:2), the viscosities of these DESs at 20°C were 2350 and 3893 mPa s, due to the low pKa of *o*-DHB ($pK_{a1} = 9.34$, $pK_{a2} = 12.6$ in H_2O, 25°C)[53] and high pKa of m-DHB ($pK_{a1} = 9.32$, $pK_{a2} = 11.1$ in H_2O, 25°C).[53] Moreover, the increase in the molar ratio of HBD in DES leads to the decrease in the viscosity of DES. For example, the viscosities of [CMPyH][$CuCl_2$]:*o*-DHB (1:1), [CMPyH][$CuCl_2$]:*o*-DHB (1:1.5), and [CMPyH][$CuCl_2$]:*o*-DHB (1:2) at 20°C were measured to be 4806, 3442, and 2350 mPa s, respectively.

3.2 | CO absorption

3.2.1 | Effects of different CO partial pressures and absorption temperatures

These cooperative DESs were easily prepared by equimolar mixing [CMPyH][Cl] with copper(I) chloride (CuCl), and then mixing with diol compounds (*o*-DHB, *m*-DHB, EG, and PD) at different molar ratios

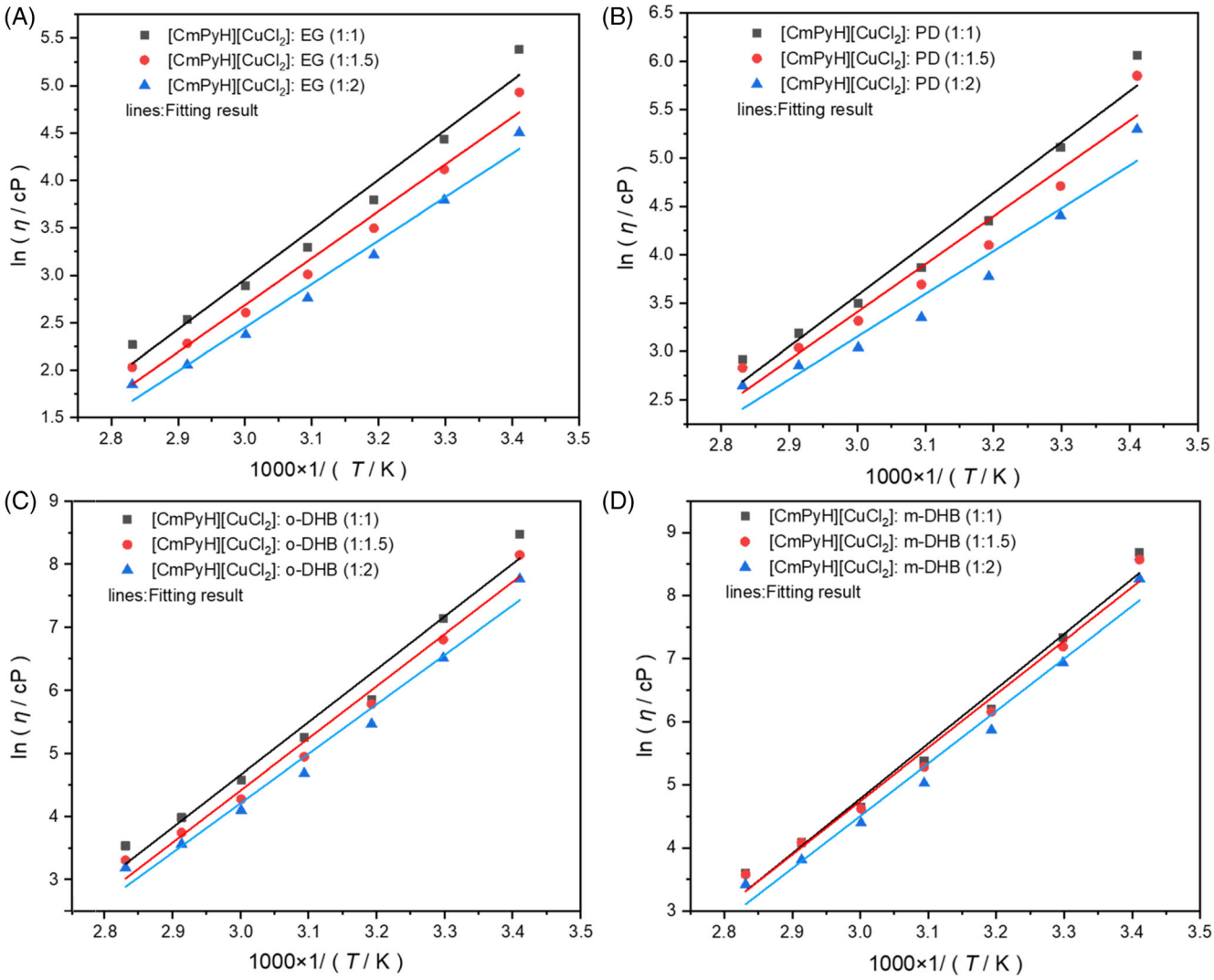

FIGURE 4 Linear relationship of lnη vs. $1/T$ for deep eutectic solvents with different hydrogen-bond donors. (A) Ethylene glycol (EG), (B) 1,3-propanediol (PD), (C) *o*-dihydroxybenzene (*o*-DHB), (D) *m*-dihydroxybenzene (*m*-DHB).

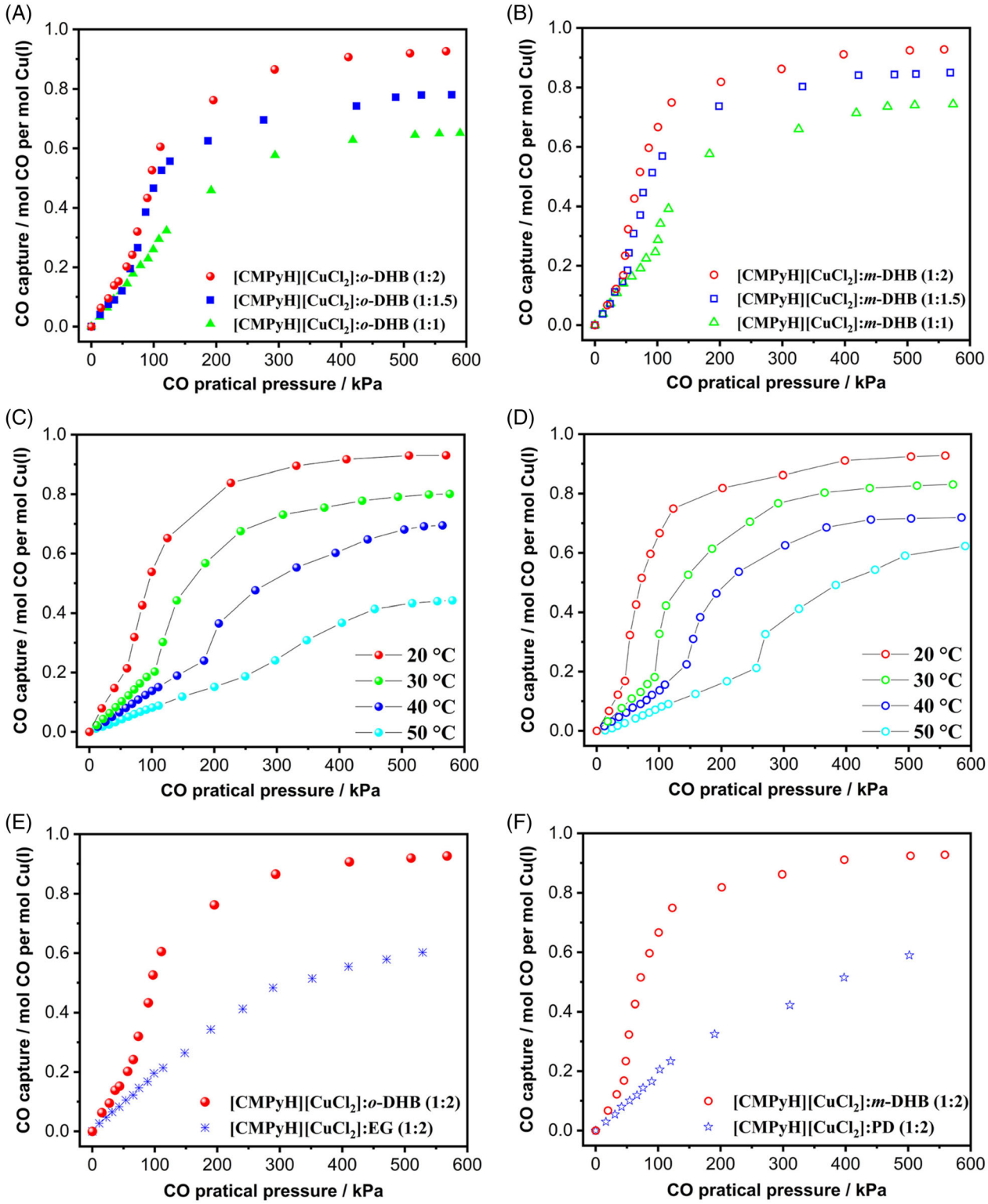

FIGURE 5 Effect of molar ratio of hydrogen-bond accepters:hydrogen-bond donors (HBA:HBD) on carbon monoxide (CO) capture by deep eutectic solvents (DESs) containing *o*-dihydroxybenzene (*o*-DHB) (A) and *m*-dihydroxybenzene (*m*-DHB) (B) at 20°C and different partial pressures. The S-shaped absorption isotherms of CO in DESs containing *o*-DHB (C) and *m*-DHB (D) at different temperatures. (E and F) Comparison of CO capture by DESs containing benzenediols and alkanediols with HBA:HBD = 1:2 at 20°C and different partial pressures. EG, ethylene glycol; PD, 1,3-propanediol.

(1:1, 1:1.5, and 1:2). The CO absorption performances under different temperatures and CO partial pressures were systematically studied, and the results were shown in Figure 5. It is shown that the molar ratios of the captured CO to Cu(I) in [CMPyH][$CuCl_2$]:*m*-DHB (1:2) at 20°C were 0.921 and 0.667 at 5 and 1 bar, respectively, suggesting that the captured CO could be facilely stripped from the CO-saturated

DESs by vacuum. Clearly, the absorption capacity decreased with the decrease of CO partial pressure (Figure 5A,B). In addition, the molar ratio of captured CO to Cu(I) was increased with the increase of HBDs in DESs. Take [CMPyH][$CuCl_2$]:*m*-DHB DESs as an example, when the molar ratios of HBA:HBD were 1:1, 1:1.5, and 1:2, the CO absorption capacities were 0.738, 0.844, and 0.921 mol CO per mol Cu(I) at 20°C and 5 bar. For [CMPyH][$CuCl_2$]:*o*-DHB DESs, the CO absorption capacities were 0.710, 0.774, and 0.920 mol CO per mol Cu(I) for 1:1, 1:1.5, and 1:2, respectively. The lower CO absorption capacities of DESs with *o*-DHB as the HBD were due to the lower acidity of *o*-DHB ($pK_{a1} = 9.34$, $pK_{a2} = 12.6$ in H_2O, 25°C).[53] However, CO capacities of DESs with benzenediols were higher than those of DESs with alkanediols (Figure 5E,F). Furthermore, the CO capacities of benzenediol-containing DESs with a molar ratio of HBA:HBD = 1:2 were determined under different absorption temperatures (Figure 5C,D). It can be seen that the CO capacity decreased when the temperature was increased. For example, the CO absorption capacity of [CMPyH][$CuCl_2$]:*o*-DHB (1:2) decreased from 0.920 to 0.70 mol CO per mol Cu(I) when the temperature was increased from 20 to 40°C at 5 bar. Considering the viscosity of [CMPyH][$CuCl_2$]:*o*-DHB (1:2) decreased dramatically from 2350 at 20°C to 235.9 mPa s at 40°C (reduced by 90%) while the CO absorption capacity reduced by only 24%, these viscous DESs could be handled in industrial processes. The results also suggested that the captured CO could be facilely stripped from the CO-saturated DESs by heating.

Interestingly, the S-shaped absorption isotherms were obtained and showed in Figure 5C,D, where the amount of CO adsorbed would be small at low pressures but rise sharply just before the pressure reaches the desired absorption pressure. Here, the "desired absorption pressure" and the "characteristic threshold 'gate-opening' pressure" have the same meaning—when this pressure is reached, the adsorption capacity increases sharply. It can be seen from Figure 5

TABLE 4 Carbon monoxide (CO) capture capacities (in mol CO per mol Cu^+) of typical deep eutectic solvents, ionic liquids, and organic solvents.

Absorbent	*T* (°C)	Capacity (mol CO/mol Cu^+) 1 bar	2 bar	5 bar	Ref.
[CMPyH][$CuCl_2$]:*m*-DHB (1:2)	20	0.667	0.819	0.921	This work
[CMPyH][$CuCl_2$]:*m*-DHB (1:1.5)	20	0.541	0.742	0.844	This work
[CMPyH][$CuCl_2$]:*m*-DHB (1:1)	20	0.287	0.590	0.738	This work
[CMPyH][$CuCl_2$]:*o*-DHB (1:2)	20	0.540	0.772	0.920	This work
[CMPyH][$CuCl_2$]:*o*-DHB (1:1.5)	20	0.465	0.643	0.774	This work
[CMPyH][$CuCl_2$]:*o*-DHB (1:1)	20	0.241	0.476	0.710	This work
[CMPyH][$CuCl_2$]:PD (1:2)	20	0.201	0.342	0.590	This work
[CMPyH][$CuCl_2$]:EG (1:2)	20	0.198	0.365	0.587	This work
[HBDMAEE-C_6][Cu_2Cl_3]$_2$	40	0.063	0.36	–	52
[HTMPDA-C_6][Cu_2Cl_3]$_2$	40	0.032	0.092	–	52
[HTMHDA-C_6][Cu_2Cl_3]$_2$	40	0.059	0.13	–	52
[HTMHDA-DE][Cu_2Cl_3]$_2$	40	0.038	0.087	–	52
[HTMHDA-TE][Cu_2Cl_3]$_2$	40	0.060	0.16	–	52
[HDEEA][$CuCl_2$]:EG (1:4)	20	0.203	0.348	0.564	51
[HDEEA][$CuCl_2$]:EG (1:2)	20	0.161	0.276	0.482	51
[HDEEA][$CuCl_2$]:EG (1:1)	20	0.140	0.215	0.402	51
[EimH][OAc]-0.6CuOAc	20	0.45	0.50	–	57
[Emim][OAc]-0.6CuOAc	20	0.07	–	–	57
[TEA][$CuCl_2$]	30	0.078	0.174	0.609	49
[TPA][$CuCl_2$]	30	0.106	0.185	0.783	49
[EimH][$CuCl_2$]	20	0.157	0.310	–	50
[EimH][$CuCl_2$]	30	0.118	0.236	–	50
[BimH][$CuCl_2$]	30	0.111	0.234	–	50
[HimH][$CuCl_2$]	30	0.105	0.229	–	50
[BimH][$CuCl_2$]-1.0$ZnCl_2$	80	0.075	0.128	0.338	47
[BimH][$CuCl_2$]	80	0.027	–	–	47
[BimH][$ZnCl_3$]	80	0.006	–	–	47
[Hmim][$CuCl_2$]	30	0.02	–	–	58

Abbreviations: EG, thylene glycol; *m*-DHB, *m*-dihydroxybenzene; *o*-DHB, *o*-dihydroxybenzene; PD, 1,3-propanediol.

that there is a dramatic increase in absorption capacity after about 0.2 mol CO per mol Cu(I) captured in DESs with preorganized benzenediols as the HBDs, and the desired absorption pressure for these DESs are different under different molar ratio of HBA:HBD and different absorption temperatures. For example, it can be seen from Figure 5C that the "gate-opening" pressures for CO absorption in [CMPyH][$CuCl_2$]:*o*-DHB (1:2) at 20, 30, 40, and 50°C were measured to be 56, 105, 140, and 250 kPa. Additionally, these absorption isotherms are different from the classical Langmuir-type absorption isotherms of CO in DESs with alkanediols as HBDs,[51] where the amount of CO adsorbed increases continuously, but at a decreasing rate, as the pressure is raised (Figure 5E,F). According to the previous reports, the S-shaped absorption isotherm is beneficial to gas storage.[54,55] These stepwise curves are the result of the combination of physical adsorption and chemical adsorption, and the chemical adsorption becomes the dominant factor when CO partial pressure reaches the desired absorption pressure, the similar results can be found in the SO_2 capture by DESs[56] and CO capture by ILs.[49]

We selected some typical Cu(I)-based DESs and ILs to compare the capture capacity and Cu(I) efficiency in mol CO per mol Cu^+ (Table 4). It can be seen that the DESs with preorganized benzenediols as the HBDs reported in this work showed high CO capture capacity and Cu(I) efficiency among these solvents.

3.2.2 | Cycles of CO_2 absorption

In separation processes, the reversibility of separation agents is one of the essential aspects as it controls the economy of separation and purification technology. Thus, besides the high efficiency of Cu(I) and high capacity of CO, the CO absorption–desorption recycling property of these Cu(I)-based benzenediol-containing DESs was also investigated, and the results of CO absorption–desorption cycles of [CMPyH][$CuCl_2$]:*o*-DHB (1:2) are shown in Figure 6. Overall, all of the CO capture capacities of [CMPyH][$CuCl_2$]:*o*-DHB (1:2) at typical CO partial pressures remained steady during these cycles, indicating that the CO capture process by Cu(I)-based DESs with benzenediols as the HBDs is highly reversible and energy-saving. Although the long-term stability and recyclability of Cu(I)-based benzenediol-containing DESs remain to be tested over many more CO absorption–desorption cycles under atmospheric pressures, these initial results indicate that these DESs with benzenediols as HBDs are remarkably robust.

3.3 | Mechanism of CO absorption

3.3.1 | FT-IR analysis

The mechanism of CO capture by [CMPyH][$CuCl_2$]:*o*-DHB (1:2) was further studied and characterized by FT-IR spectroscopy (Figure 7). Figure 7A shows the FT-IR results of [CMPyH][$CuCl_2$]:*o*-DHB (1:2) before CO absorption, after CO absorption, and after CO desorption. It can be seen that, compared with neat DES, a new peak at

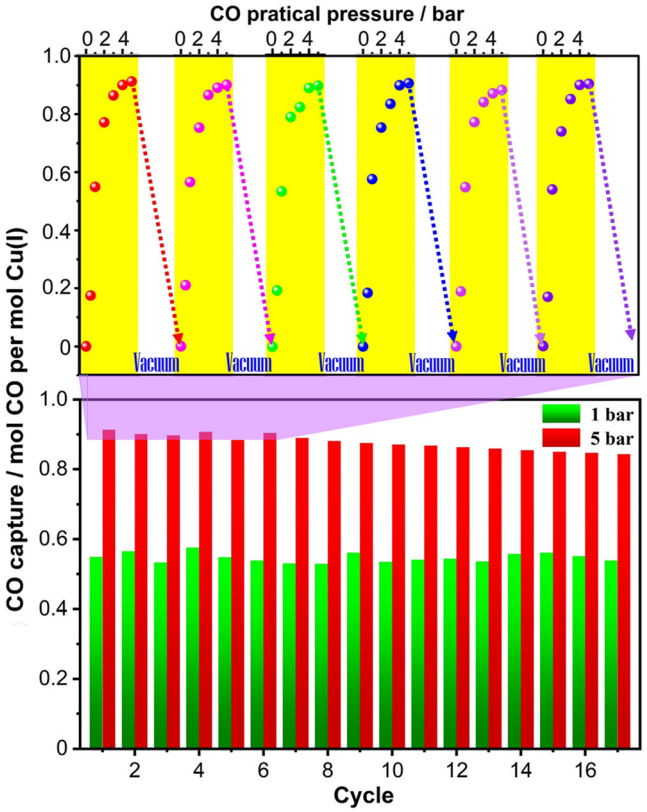

FIGURE 6 Seventeen consecutive carbon monoxide (CO) absorption–desorption cycles over [CMPyH][$CuCl_2$]:*o*-DHB (1:2). CO absorptions were carried out at 20°C under different partial pressures of CO, and the reversible chemical adducts $[Cu_2Cl_4 + 2CO]^{2-}$ may form during CO absorption by these deep eutectic solvents. Desorption was performed at 80°C under vacuum. *o*-DHB, *o*-dihydroxybenzene.

2099 cm^{-1} was occurred after the absorption of CO at 20°C and 5 bar, indicating the interaction between CO and Cu(I). The peak disappeared after the desorption of CO. The results indicated the formation of copper(I)-carbonyl chemical adduct was reversible, which is similar to the results reported by Repper et al.[59] Because of the formation of $[CuCl_2]^-$ dimer was energetically favored,[50] it is inferred that the reversible chemical adducts $[Cu_2Cl_4 + 2CO]^{2-}$ were formed during CO absorption by these DESs. In addition, the performances of CO capture by [CMPyH][$CuCl_2$]:*o*-DHB DESs with different molar ratios of HBD:HBA were also investigated by FT-IR spectroscopy, and the peak change is shown in Figure 7B. With the increasing molar ratio of HBD:HBA in these DESs from 1:1 to 1:2, the typical stretching vibration peak of CO slightly blue-shifted from 2094 to 2099 cm^{-1}, after the gradual increasing absorption capacity from 0.738 to 0.921 mol CO per mol Cu(I). Interestingly, the ratio of the blue-shifted CO peak and the capacity of CO absorption are increased linearly as the molar ratio of HBD:HBA increased (Figure 7D). For another comparison, FT-IR results of [CMPyH][$CuCl_2$]:EG DESs with different molar ratios of HBD:HBA after CO absorption are also shown in Figure 7C. It can be seen that with the increasing molar ratio of HBD:HBA and the increasing CO capacity (Figure 7E), the

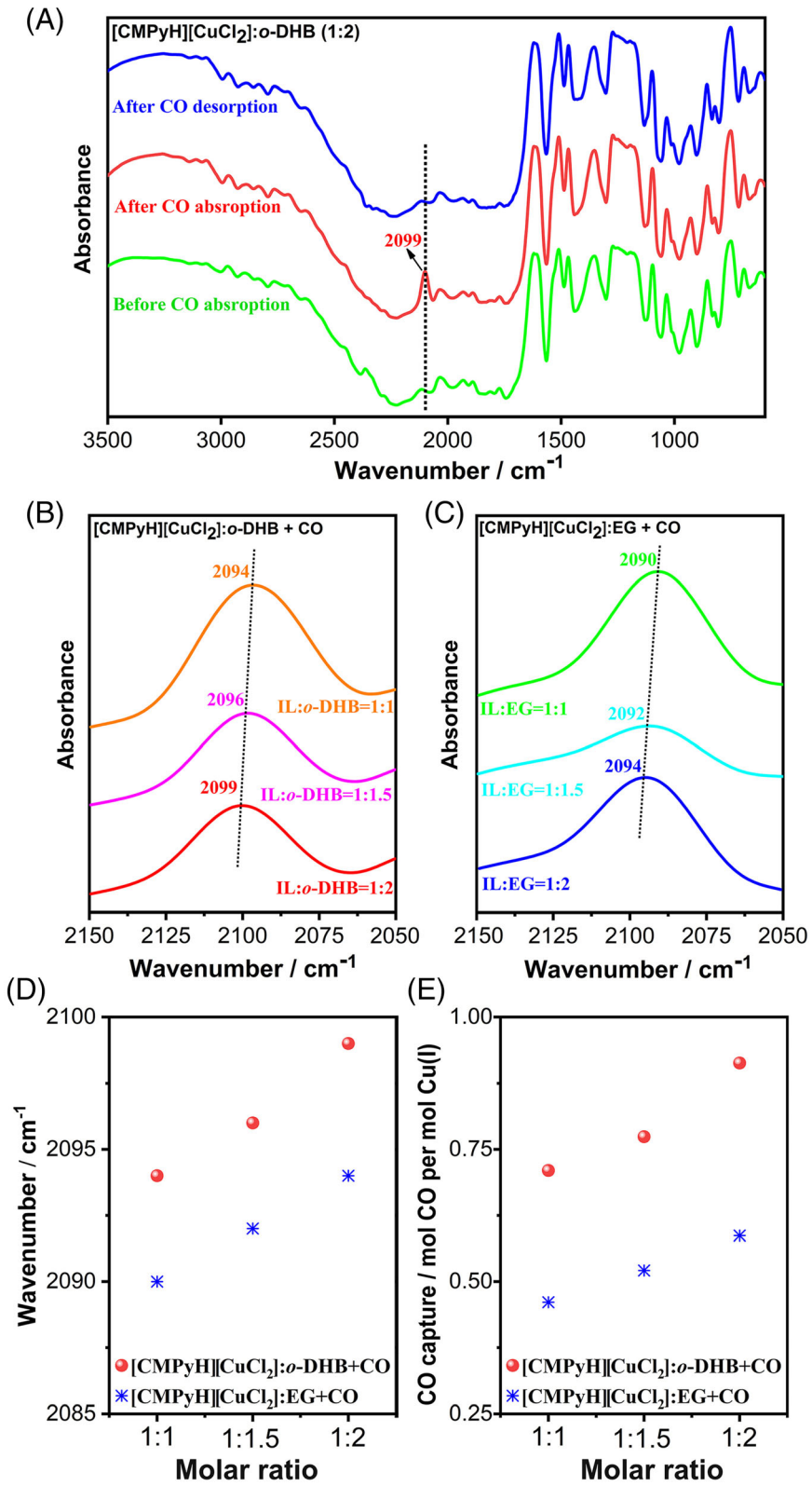

FIGURE 7 Fourier transform infrared spectrometer spectra of [CMPyH][$CuCl_2$]:*o*-DHB and [CMPyH][$CuCl_2$]:EG deep eutectic solvents before and after the absorption of carbon monoxide (CO) at 20°C and 5 bar. (A) Spectra of [CMPyH][$CuCl_2$]:*o*-DHB (1:2) before CO absorption, after CO absorption, and after CO desorption; (B and C) comparison of the typical CO peak in the spectra of [CMPyH][$CuCl_2$]:*o*-DHB and [CMPyH][$CuCl_2$]:EG with different molar ratios of hydrogen-bond accepters:hydrogen-bond donors (HBA:HBD) after CO absorption; (D) relationship between wavenumbers of the CO peak with the molar ratio of HBA:HBD; (E) relationship between CO capture capacity with the molar ratio of HBA:HBD. EG, ethylene glycol; IL, ionic liquids; *o*-DHB, *o*-dihydroxybenzene.

stretching vibration peak of CO also slightly blue-shifted from 2090 to 2094 cm^{-1}. Furthermore, with the same molar ratio of HBD:HBA in both [CMPyH][$CuCl_2$]:EG and [CMPyH][$CuCl_2$]:*o*-DHB, the blue-shifted peak of CO could be observed from the FT-IR spectroscopy of [CMPyH][$CuCl_2$]:EG + CO to that of [CMPyH][$CuCl_2$]:*o*-DHB + CO (Figure 7D). For example, with the molar ratio of HBD:HBA = 1:2, the

stretching vibration peaks of CO for [CMPyH][$CuCl_2$]:EG + CO and [CMPyH][$CuCl_2$]:*o*-DHB + CO were 2094 and 2099 cm^{-1}, respectively, indicating the strong coordination of Cu(I)···CO in CO-saturated [CMPyH][$CuCl_2$]:*o*-DHB DESs, which originally arose from the strong acidity of benzenediols. These results indicated that the high CO capture capacity could be obtained by DESs with preorganized benzenediols as the HBDs.

3.3.2 | NMR analysis

Moreover, benzenediols are beneficial to CO capture by Cu(I)-based DESs, which can also be proved by NMR. Figure 8 shows the comparison of ^{13}C NMR spectra results of [CMPyH][$CuCl_2$]:*o*-DHB (1:2) and [CMPyH][$CuCl_2$]:EG (1:2) before and after the CO absorption. From the comparison of the ^{13}C NMR spectra of [CMPyH][$CuCl_2$]:*o*-DHB (1:2) before and after the absorption of CO, it can be seen that the typical resonances at about $\delta = 110.2$, 114.0, and 139.6 ppm in the spectrum of neat [CMPyH][$CuCl_2$]:*o*-DHB (1:2), which can be assigned to the *o*-DHB carbon atoms, were moved down-field to $\delta = 111.8$, 115.5, and 141.2 ppm in the spectrum of CO-saturated [CMPyH][$CuCl_2$]:*o*-DHB (1:2), indicating that the strong hydrogen bonds played an important role in the capture of CO by DESs with benzenediol as HBDs and the formation of coordination bonds between Cu(I) and CO.[50] Take the ^{13}C NMR spectra of [CMPyH][$CuCl_2$]:EG (1:2) before and after the absorption of CO for comparison; the typical resonance at about $\delta = 57.7$ ppm in the spectrum of neat DES, assigning to the EG carbon atoms, was slightly moved up-field to $\delta = 57.1$ ppm in the spectrum of CO-saturated DES, indicating the formation of weak hydrogen bonds of EG in the CO capture by DESs with EG as HBDs. It is surprising that no other resonances were observed in Figure 8, especially the resonance for CO, although the high CO capture capacities of DESs were obtained. The reason for this phenomenon may be attributed to the very low mass fraction of CO in [CMPyH][$CuCl_2$]:*o*-DHB (1:2) and [CMPyH][$CuCl_2$]:EG (1:2) in d_6-DMSO. A similar phenomenon can be found in the literatures.[49,51]

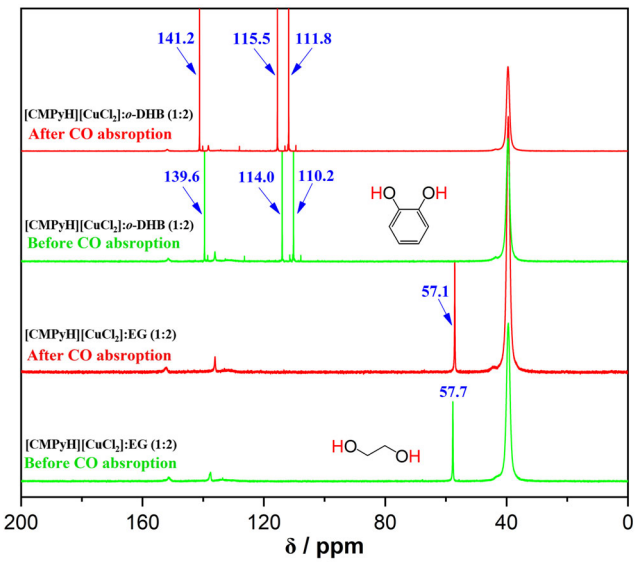

FIGURE 8 ^{13}C Nuclear magnetic resonance spectrometer spectra of [CMPyH][$CuCl_2$]:*o*-DHB (1:2) and [CMPyH][$CuCl_2$]:EG (1:2) deep eutectic solvents (hydrogen-bond accepters:hydrogen-bond donors = 1:2) before and after the absorption of carbon monoxide (CO) at 20°C and 5 bar. EG, ethylene glycol; *o*-DHB, *o*-dihydroxybenzene.

3.3.3 | Density functional theory calculations

Density functional theory (DFT) calculations at B3LYP/6-31G++(d,p) level with Gaussian 16[60] were used to compare the reactions of CO with active Cu(I) sites of $[Cu_2Cl_4]^{2-}$, the dimer anion of [$CuCl_2$], in DESs with different diol HBDs, *m*-DHB and PD as the examples (molar ratio of HBA:HBD = 1:1). Figure 9 shows the optimized structures of $[Cu_2Cl_4]^{2-}$, *m*-DHB···$[Cu_2Cl_4]^{2-}$···*m*-DHB, and PD···$[Cu_2Cl_4]^{2-}$···PD. It is confirmed by DFT calculation that the interaction between the linear isolated anion $[CuCl_2]^-$ and CO is weak ($\Delta H = -21.1$ kJ mol^{-1}), while the planar dimer anion $[Cu_2Cl_4]^{2-}$ has more negative interaction enthalpy of −52.1 and −50.4 kJ mol^{-1}. Thus, it is supposed that the formation of dimer anion $[Cu_2Cl_4]^{2-}$ is beneficial to CO capture. It can be seen from Figure 9 that the dimer anion $[Cu_2Cl_4]^{2-}$ has two three-coordinated Cu(I) atoms, and all six atoms are in the same plane. The optimized structures of the planar conformation for the complex *m*-DHB···$[Cu_2Cl_4]^{2-}$···*m*-DHB, including two *m*-DHB molecules, are clearly shown. Differently, the optimized structure of the chair conformation is obtained for the complex PD···$[Cu_2Cl_4]^{2-}$···PD. Additionally, the calculated terminal Cl−Cu−bridged Cl angles in $[CuCl_2]^-$, $[Cu_2Cl_4]^{2-}$, *m*-DHB···$[Cu_2Cl_4]^{2-}$···*m*-DHB, and PD···$[Cu_2Cl_4]^{2-}$···PD were 180.0°, 133.9°, 151.4°, and 162.9°, respectively. It is clear that the Cl−Cu−Cl angle in $[CuCl_2]^-$ bends a lot in the complex *m*-DHB···$[Cu_2Cl_4]^{2-}$···*m*-DHB and $[Cu_2Cl_4]^{2-}$, while it bends a little in the complex PD···$[Cu_2Cl_4]^{2-}$···PD, indicating the strong bridge Cu···Cl interactions were formed in the formers. Furthermore, the strength of hydrogen bonds in the complexes *m*-DHB···$[Cu_2Cl_4]^{2-}$···*m*-DHB and PD···$[Cu_2Cl_4]^{2-}$···PD are different. The distances between H of –OH and terminal Cl in *m*-DHB···$[Cu_2Cl_4]^{2-}$···*m*-DHB (2.154 and 2.200 Å) are shorter than those in PD···$[Cu_2Cl_4]^{2-}$···PD (2.328 and 2.369 Å), due to the stronger acidity of preorganized *m*-DHB ($pK_{a1} = 9.32$, $pK_{a2} = 11.1$ in H_2O, 25°C)[53] than PD ($pK_a = 16.3$).[61] The relatively strong –OH···Cl hydrogen bonds can weaken the terminal Cu–Cl bond, leading to more ligands connecting to Cu(I). As a result, the interaction between CO and Cu(I) in *m*-DHB···$[Cu_2Cl_4]^{2-}$···*m*-DHB is stronger than that in PD···$[Cu_2Cl_4]^{2-}$···PD.

To further investigate the reaction between the active Cu(I) site and CO, the structures of the complexes of *m*-DHB···$[Cu_2Cl_4]^{2-}$···*m*-DHB and PD···$[Cu_2Cl_4]^{2-}$···PD with one CO and two CO are also calculated by DFT, and the results are shown in Figure 9. It can be seen that when Cu(I) interacts with CO, the planar three-coordination conformation of <$CuCl_3$> transfers to the tetrahedral four-coordination conformation of <$CuCl_3CO$>. It is interesting that the planarization of

the bowl-shaped complex *m*-DHB···$[Cu_2Cl_4 + CO]^{2-}$···*m*-DHB to *m*-DHB···$[Cu_2Cl_4 + 2CO]^{2-}$···*m*-DHB occurs by the reaction with another CO. The interaction enthalpies between the complex *m*-DHB···$[Cu_2Cl_4]^{2-}$···*m*-DHB and CO are calculated to be $\Delta H_1 = -56.8$ kJ mol^{-1} and $\Delta H_2 = -53.7$ kJ mol^{-1}, respectively. The negative values of ΔH indicate the exothermic absorption process as well as the strong chemical interaction between CO and the complex *m*-DHB···$[Cu_2Cl_4]^{2-}$···*m*-DHB ($|\Delta H|$ >50 kJ mol^{-1}). Thus, up to equimolar absorption capacity could be reached by DES with *m*-DHB as the HBD. For comparison, the interaction enthalpies between the complex PD···

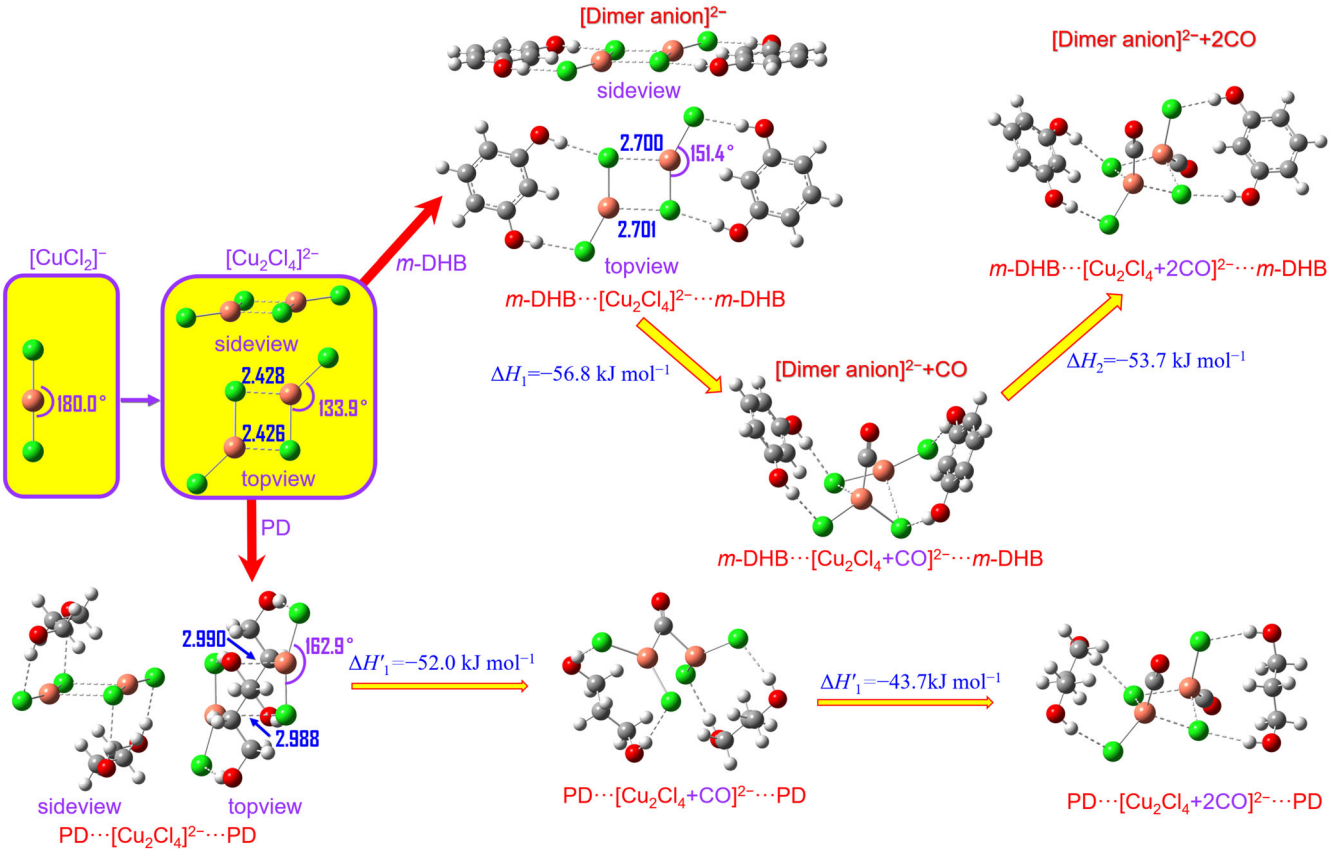

FIGURE 9 Optimized structures of $[Cu_2Cl_4]^{2-}$, *m*-DHB···$[Cu_2Cl_4]^{2-}$···*m*-DHB, PD···$[Cu_2Cl_4]^{2-}$···PD, and the complexes with carbon monoxide (CO). Note that van der Waals radii (in Å)[62] are 1.70 (C), 1.20 (H), 1.52 (O), 1.75 (Cl), and 1.40 (Cu), respectively. *m*-DHB, *m*-dihydroxybenzene; PD, 1,3-propanediol.

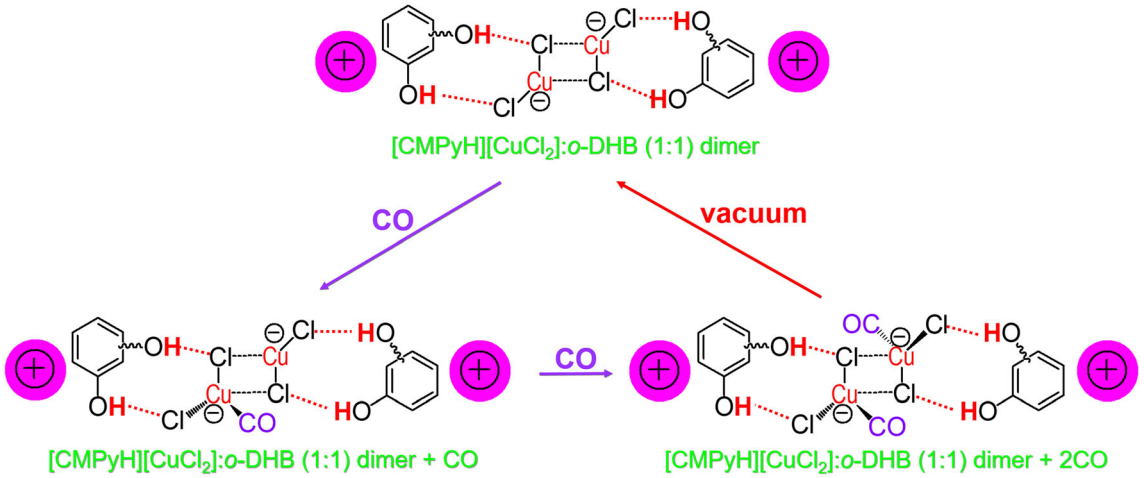

FIGURE 10 Possible mechanism of carbon monoxide (CO) absorption by deep eutectic solvents with preorganized *o*-dihydroxybenzene (*o*-DHB) as hydrogen-bond donors through cooperation of hydrogen bonding and coordination.

$[Cu_2Cl_4]^{2-}\cdots$PD and CO are calculated to be $\Delta H'_1 = -52.0$ kJ mol^{-1} and $\Delta H'_2 = -43.7$ kJ mol^{-1}, respectively. Interestingly, the interaction enthalpy for the optimized complex PD$\cdots[Cu_2Cl_4 + CO]^{2-}\cdots$PD is high due to the cooperation of Cu−CO−Cu. The results indicate that more than 0.5 mol CO per mol Cu(I) could be captured by DES with PD as the HBD. However, it is clear that the efficiency of Cu(I) in DES with *m*-DHB is higher than that in DES with PD due to the strong cooperation of –OH$\cdots$Cl hydrogen bonding and Cu$\cdots$CO coordination, which originates from the strong acidity of preorganized *m*-DHB.

Based on the above discussion, the plausible mechanism of CO absorption by DESs with preorganized *o*-DHB as HBDs can be proposed as described in Figure 10.

4 | CONCLUSIONS

In summary, a new absorption strategy based on cuprous ionic liquid engineering combined with preorganized HBDs has been developed to form a series of functional DESs for enhanced CO capture via promoting cooperation. Thus, up to 0.667 and 0.921 mol CO per mol Cu(I) could be reached by [CMPyH][$CuCl_2$]:*m*-DHB (1:2) under 1 bar or 5 bar CO, respectively. Quantum-chemical calculations and spectroscopic investigations revealed that, compared with alkanediols, benzenediols are beneficial to CO capture by Cu(I)-based DESs. Additionally, excellent reversibility (17 absorption–desorption cycles) could be reached with steady CO capacity during 0–5 bar. Thus, easy preparation of DESs, high capacity of CO, and high efficiency of Cu(I) make these preorganized DESs pave an alternative way for CO capture and conversion. We believe that the method may also open a door to achieving high efficiency of active sites as well as high capacity of gases such as NO_x, SO_2, H_2S, and CO_2 by functional materials.

AUTHOR CONTRIBUTIONS

Guokai Cui: Supervision, conceptualization, project administration, funding acquisition, investigation, formal analysis, writing—original draft, writing—review and editing. **Chengyu Ren**: Investigation, data curation, formal analysis, visualization. **Ruina Zhang**: Methodology, formal analysis, visualization. **Xing Li**: Formal analysis, validation. **Zhenzhen Yang**: Formal analysis. **Lei Zhang**: Formal analysis. **Quanli Ke**: Formal analysis, funding acquisition. **Ying Zhou**: Formal analysis, funding acquisition, resources, supervision. **Hanfeng Lu**: Conceptualization, project administration, resources, formal analysis, funding acquisition. **Sheng Dai**: Conceptualization, project administration, formal analysis, funding acquisition, writing—review and editing.

ACKNOWLEDGMENTS

This work was financially supported by the Key Research and Development Project in Zhejiang Province (no. 2024C03108, 2023C03127, and 2024C03114), the National Natural Science Foundation of China (no. 22378353 and 22208300), the Zhejiang Provincial Natural Science Foundation of China (no. LTGS24E080008), and the Zhejiang Provincial Postdoctoral Science Foundation (no. ZJ2023145). Sheng Dai was supported financially by the Division of Chemical Sciences, Geosciences, and Biosciences, Office of Basic Energy Sciences, US Department of Energy.

CONFLICT OF INTEREST STATEMENT

The authors have no conflict of competing interests.

DATA AVAILABILITY STATEMENT

The data that supports the findings of this study are available in Supporting Information S1 and S2 of this article.

ORCID

Guokai Cui https://orcid.org/0000-0002-7223-2869
Hanfeng Lu https://orcid.org/0000-0001-8934-8270
Sheng Dai https://orcid.org/0000-0002-8046-3931

REFERENCES

1. Shi Y, Hu Y-F, Ye J, et al. Stabilization of Pd0 by Cu alloying: theory-guided design of Pd3Cu electrocatalyst for anodic methanol carbonylation. *Angew Chem Int Ed*. 2024;63(25):e202401311.
2. Wang X, Chen Y, Li F, et al. Site-selective protonation enables efficient carbon monoxide electroreduction to acetate. *Nat Commun*. 2024;15(1):616.
3. Parker AL, Johnstone TC. Carbon monoxide poisoning: a problem uniquely suited to a medicinal inorganic chemistry solution. *J Inorg Biochem*. 2024;251:112453.
4. Zhang X-W, Wang C, Mo Z-W, Chen X-X, Zhang W-X, Zhang J-P. Quasi-open Cu(i) sites for efficient CO separation with high O_2/H_2O tolerance. *Nat Mater*. 2024;23(1):116-123.
5. Ma X, Albertsma J, Gabriels D, et al. Carbon monoxide separation: past, present and future. *Chem Soc Rev*. 2023;52(11):3741-3777.
6. Ramírez-Santos ÁA, Castel C, Favre E. A review of gas separation technologies within emission reduction programs in the iron and steel sector: current application and development perspectives. *Sep Purif Technol*. 2018;194:425-442.
7. Jouny M, Luc W, Jiao F. High-rate electroreduction of carbon monoxide to multi-carbon products. *Nat Catal*. 2018;1(10):748-755.
8. Zhou T, Gui C, Sun L, et al. Energy applications of ionic liquids: recent developments and future prospects. *Chem Rev*. 2023;123(21):12170-12253.
9. Yu G, Dai C, Liu N, Xu R, Wang N, Chen B. Hydrocarbon extraction with ionic liquids. *Chem Rev*. 2024;124(6):3331-3391.
10. Zhang R, Ke Q, Zhang Z, Zhou B, Cui G, Lu H. Tuning functionalized ionic liquids for CO_2 capture. *Int J Mol Sci*. 2022;23(19):11401.
11. Matuszek K, Piper SL, Brzęczek-Szafran A, et al. Unexpected energy applications of ionic liquids. *Adv Mater*. 2024;36(23):2313023.
12. Hansen BB, Spittle S, Chen B, et al. Deep eutectic solvents: a review of fundamentals and applications. *Chem Rev*. 2021;121(3):1232-1285.
13. Hu M, Han B, Xie L, et al. Ultrasonic assisted natural deep eutectic solvents as a green and efficient approach for extraction of hydroxytyrosol from olive leaves. *Ind Chem Mater*. 2024;2(2):309-320.
14. Chen Y, Han X, Liu Z, Yu D, Guo W, Mu T. Capture of toxic gases by deep eutectic solvents. *ACS Sustain Chem Eng*. 2020;8(14):5410-5430.
15. Chen K, Shi G, Zhou X, Li H, Wang C. Highly efficient nitric oxide capture by azole-based ionic liquids through multiple-site absorption. *Angew Chem Int Ed*. 2016;55(46):14364-14368.
16. Lv X, Chen K, Shi G, et al. Design and tuning of ionic liquid–based HNO donor through intramolecular hydrogen bond for efficient inhibition of tumor growth. *Sci Adv*. 2020;6(45):eabb7788.

17. Liu J, Xu Y. NOx absorption and conversion by ionic liquids. *J Hazard Mater*. 2021;409:124503.
18. Huang Y, Cui G, Zhao Y, et al. Preorganization and cooperation for highly efficient and reversible capture of low-concentration CO_2 by ionic liquids. *Angew Chem Int Ed Engl*. 2017;56(43):13293-13297.
19. Chen F-F, Huang K, Zhou Y, et al. Multi-molar absorption of CO_2 by the activation of carboxylate groups in amino acid ionic liquids. *Angew Chem Int Ed Engl*. 2016;55(25):7166-7170.
20. Suo X, Fu Y, Do-Thanh C-L, et al. CO_2 chemisorption behavior in conjugated carbanion-derived ionic liquids via carboxylic acid formation. *J Am Chem Soc*. 2022;144(47):21658-21663.
21. Xu Y, Zhang R, Zhou Y, et al. Tuning ionic liquid-based functional deep eutectic solvents and other functional mixtures for CO_2 capture. *Chem Eng J*. 2023;463:142298.
22. Wang K, Zhang Z, Wang S, Jiang L, Li H, Wang C. Dual-tuning azole-based ionic liquids for reversible CO_2 capture from ambient air. *ChemSusChem*. 2024;17(16):e202301951.
23. Sun X, Zeng S, Li G, et al. Selective CO2 separation through physicochemical absorption by triazole-functionalized ionic liquid binary absorbents. *AIChE J*. 2024;70(5):e18376.
24. Chen M, Xiong W, Chen W, Li S, Zhang F, Wu Y. Synergy of carbanion siting and hydrogen bonding in super-nucleophilic deep eutectic solvents for efficient CO_2 capture. *AIChE J*. 2024;70(4):e18319.
25. Qiu L, Li B, Hu J, et al. Cascade CO_2 insertion in carbanion ionic liquids driven by structure rearrangement. *J Am Chem Soc*. 2024;146(43):29588-29598.
26. Cui G, Cheng Y, Zhang W, et al. Highly efficient CO_2 capture from open air and dilute gas streams by tunable azolate ionic liquids based deep eutectic solvents. *Chem Eng J*. 2025;505:159193.
27. Cui G, Xu Y, Hu D, et al. Tuning functional ionic deep eutectic solvents as green sorbents and catalysts for highly efficient capture and transformation of CO_2 to quinazoline-2,4(1*H*,3*H*)-dione and its derivatives. *Chem Eng J*. 2023;469:143991.
28. Cui G, Zheng J, Luo X, et al. Tuning anion-functionalized ionic liquids for improved SO_2 capture. *Angew Chem Int Ed*. 2013;52(40):10620-10624.
29. Zhang P, Xiong W, Shi M, et al. Natural deep eutectic solvent-based gels with multi-site interaction mechanism for selective membrane separation of SO_2 from N_2 and CO_2. *Chem Eng J*. 2022;438:135626.
30. Scaglione N, Wylie L, Padua A, Costa Gomes M. Improved reversible and selective SO_2 absorption by a stable phosphonium carboxylate ionic liquid. *ACS Sustain Chem Eng*. 2024;12(28):10486-10497.
31. Liu P, Cai K, Zhang X, Zhao T. Effective absorption of SO_2 by imidazole-based protic ionic liquids with multiple active sites: thermodynamic and mechanical studies. *AIChE J*. 2022;68(4):e17596.
32. Zhang P, Tu Z, Zhang X, Hu X, Wu Y. Acidic protic ionic liquid-based deep eutectic solvents capturing SO with low enthalpy changes. *AIChE J*. 2023;69(9):e18145.
33. Zhang R, Tang L, Ge C, et al. Functional ionic liquids for SO_2 capture and conversion. *New J Chem*. 2025;49(23):9552-9571.
34. Cui G, Lyu S, Zhang F, et al. Tuning ionic liquids with functional anions for SO_2 capture through simultaneous cooperation of N and O chemical active sites with SO_2. *Ind Eng Chem Res*. 2020;59(49):21522-21529.
35. Luo X, Qiu R, Chen X, Pei B, Lin J, Wang C. Reversible construction of ionic networks through cooperative hydrogen bonds for efficient ammonia absorption. *ACS Sustain Chem Eng*. 2019;7(11):9888-9895.
36. Sun X, Li G, Zeng S, Yuan L, Bai L, Zhang X. Ultra-high NH_3 absorption by triazole cation-functionalized ionic liquids through multiple hydrogen bonding. *Sep Purif Technol*. 2023;307:122825.
37. Li K, Zong K, Wang X, Cui G, Deng D. Ionic liquids and deep eutectic solvents for NH_3 absorption and separation: a review. *New J Chem*. 2023;47(46):21426-21445.
38. Tu W, Zeng S, Bai Y, Zhang X, Dong H, Zhang X. Theoretical insights into NH_3 absorption mechanisms with imidazolium-based protic ionic liquids. *Ind Chem Mater*. 2023;1(2):262-270.
39. Huang K, Cai D-N, Chen Y-L, Wu Y-T, Hu X-B, Zhang Z-B. Thermodynamic validation of 1-alkyl-3-methylimidazolium carboxylates as task-specific ionic liquids for H_2S absorption. *AIChE J*. 2013;59(6):2227-2235.
40. Zhang X, Xiong W, Peng L, Wu Y, Hu X. Highly selective absorption separation of H_2S and CO_2 from CH_4 by novel azole-based protic ionic liquids. *AIChE J*. 2020;66(6):e16936.
41. Zhou Z, Zhang P, Chang Y, Chen X. Highly efficient capture and removal of H_2S by multi-amine functionalized ionic liquids. *J Mol Liq*. 2023;392:123501.
42. Li F, Laaksonen A, Zhang X, Ji X. Rotten eggs revaluated: ionic liquids and deep eutectic solvents for removal and utilization of hydrogen sulfide. *Ind Eng Chem Res*. 2022;61(7):2643-2671.
43. Wang B, Xie X, Wan L, Zhao W, Chen Y. H_2S absorption with deep eutectic solvents: low partial pressure capture and thermodynamic analysis. *AIChE J*. 2023;69(7):e18087.
44. Schilter D. CO capture: IL's a trap! *Nat Rev Chem*. 2017;1(6):0047.
45. Ohlin CA, Dyson PJ, Laurenczy G. Carbon monoxide solubility in ionic liquids: determination, prediction and relevance to hydroformylation. *Chem Commun*. 2004;9:1070-1071.
46. Tao D-J, Chen F-F, Tian Z-Q, et al. Highly efficient carbon monoxide capture by carbanion-functionalized ionic liquids through C-site interactions. *Angew Chem Int Ed Engl*. 2017;56(24):6843-6847.
47. Tao D-J, Qu F, Li Z-M, Zhou Y. Promoted absorption of CO at high temperature by cuprous-based ternary deep eutectic solvents. *AIChE J*. 2021;67(2):e17106.
48. David OC, Zarca G, Gorri D, Urtiaga A, Ortiz I. On the improved absorption of carbon monoxide in the ionic liquid 1-hexyl-3-methylimidazolium chlorocuprate. *Sep Purif Technol*. 2012;97:65-72.
49. Tu Z-H, Zhang Y-Y, Wu Y-T, Hu X-B. Self-enhancement of CO reversible absorption accompanied by phase transition in protic chlorocuprate ionic liquids for effective CO separation from N_2. *Chem Commun*. 2019;55(23):3390-3393.
50. Liu Y-M, Tian Z, Qu F, Zhou Y, Liu Y, Tao D-J. Tuning ion-pair interaction in cuprous-based Protic ionic liquids for significantly improved CO capture. *ACS Sustain Chem Eng*. 2019;7(13):11894-11900.
51. Cui G, Jiang K, Liu H, et al. Highly efficient CO removal by active cuprous-based ternary deep eutectic solvents [HDEEA][Cl] + CuCl + EG. *Sep Purif Technol*. 2021;274:118985.
52. Peng L, Shi M, Pan Y, et al. Ultrahigh carbon monoxide capture by novel protic cuprous-functionalized dicationic ionic liquids through complexation interactions. *Chem Eng J*. 2023;451:138519.
53. Haynes WM. *Handbook of Chemistry and Physics*. 97rd ed. CRC Press; 2016.
54. Reed DA, Keitz BK, Oktawiec J, et al. A spin transition mechanism for cooperative adsorption in metal–organic frameworks. *Nature*. 2017;550(7674):96-100.
55. Shi Y, Wang Z, Li Z, et al. Anchoring LiCl in the nanopores of metal–organic frameworks for ultra-high uptake and selective separation of ammonia. *Angew Chem Int Ed*. 2022;61(47):e202212032.
56. Cui G, Liu J, Lyu S, Wang H, Li Z, Wang J. Efficient and reversible SO_2 absorption by environmentally friendly task-specific deep eutectic solvents of PPZBr + Gly. *ACS Sustain Chem Eng*. 2019;7(16):14236-14246.
57. Tao D-J, An X-C, Gao Z-T, Li Z-M, Zhou Y. Cuprous-based composite ionic liquids for the selective absorption of CO: experimental study and thermodynamic analysis. *AIChE J*. 2022;68(5):e17631.
58. Zarca G, Ortiz I, Urtiaga A. Kinetics of the carbon monoxide reactive uptake by an imidazolium chlorocuprate(I) ionic liquid. *Chem Eng J*. 2014;252:298-304.
59. Repper SE, Haynes A, Ditzel EJ, Sunley GJ. Infrared spectroscopic study of absorption and separation of CO using copper(I)-containing ionic liquids. *Dalton Trans*. 2017;46(9):2821-2828.

60. Frisch MJ, Trucks GW, Schlegel HB, et al. Gaussian 16 (revision C.01), Gaussian, Inc. 2016.
61. Bertrand P, Bonnarme V, Piccirilli A, et al. Physical and chemical assessment of 1,3 propanediol as a potential substitute of propylene glycol in refill liquid for electronic cigarettes. *Sci Rep*. 2018;8(1): 10702.
62. Bondi A. van der Waals volumes and radii. *J Phys Chem*. 1964;68(3): 441-451.

SUPPORTING INFORMATION

Additional supporting information can be found online in the Supporting Information section at the end of this article.

How to cite this article: Cui G, Ren C, Zhang R, et al. Cuprous ionic liquid engineering combined with preorganized hydrogen-bond donors for enhanced carbon monoxide capture. *AIChE J*. 2025;71(12):e70030. doi:10.1002/aic.70030